Applied Surface Science 528 (2020) 146958

Contents lists available at ScienceDirect

Applied Surface Science

journal homepage: www.elsevier.com/locate/apsusc

Production of flexible nanocomposite membranes for x-ray detectors

Ahmad I. Ayesh[a,b,*], Belal Salah[b], Rama Nawwas[c], Aldana Alyafei[c], Sara AlMansouri[c], Leena Al-Sulaiti[b]

[a] Center for Sustainable Development, Qatar University, Doha, Qatar
[b] Department of Math., Stat. and Physics, Qatar University, Doha, Qatar
[c] College of Engineering, Qatar University, Doha, Qatar

ARTICLE INFO

Keywords:
CuO
Composite membranes
PVA
Radiation detectors
Polymer-nanoparticle

ABSTRACT

Flexible membranes of poly(vinyl alcohol) (PVA) polymer and CuO nanoparticles for x-ray detection applications are reported in this work. PVA represents a polymer matrix for nanoparticles, and its flexibility and electrical conductivity are enhanced by addition of glycerol (GL) plasticizer. Nanoparticles of an average size of $6.3 \mp 2.4nm$ are produced by a solvothermal method and added to the PVA + GL solution with different concentrations. The flexible membranes are fabricated by solution casting on glass substrates. The effect of blending of PVA + GL with nanoparticles on different characteristics of the membranes including the flexibility as well as the melting, glass transition, and degradation temperatures are tested by differential scanning calorimetry, thermal gravimetric analysis, as well as both Raman and Fourier-transform infrared spectroscopy. Electrical impedance tests reveal that both dc resistance and activation energy decrease with increasing temperature as well as nanoparticle concentration. The produced membranes reveal electrical response to x-ray due to the presence of CuO nanoparticles, and this response rises with x-ray generator voltage. The results presented in this study specify that the produced membranes are easy to produce with low cost, thus, they represent potential candidates for practical applications including x-ray detection.

1. Introduction

Conductometric x-ray detectors exhibit superior sensitivity as well as high electrical response that surpass other x-ray detection technologies [1]. They are normally used to convert x-ray radiation signal into electrical current, and they are essential for medical [2], security [3], and photon facility [4] applications. Standard x-ray detectors are typically based on semiconducting inorganic materials, and they exhibit decent resolution and wide range of detection. Yet, standard inorganic x-ray detectors have few drawbacks such as their high fabrication cost on large scale and their fragileness. Organic semiconducting membranes represent an alternative potential replacement for the standard inorganic x-ray detectors [5–7] as well as other electronic devices [8–11]. Organic membranes hold many superior advantages including low power consumption that increase their life-time, flexibility, and practical production procedure on large scale with rational cost [9].

Poly(vinyl alcohol) (PVA) is a novel biodegradable polymer with many attractive features including the controllable biodegradation rate and mechanical properties, hydrophilic nature, and biocompatibility with negligible toxicity [12]. Those features facilitated its utilization for different device and medical applications [9,12,13]. Glycerol is known as a plasticizer and its addition to a PVA membrane increases the flexibility of the end product [14]. Herein, blending PVA with glycerol decreases the intermolecular forces which increases the flexibility of the PVA polymer chains, decreases the range of interactions between stacks (edge–edge) that enables better utilization of PVA as a filler, it reduces the amount of swelled water by PVA because it reduces the surface energy of PVA, and it can enhance electrical conductivity of a PVA membrane [15].

Nanoparticles are grains of single or composite atoms with the size in the nanometer range. They have unique novel properties due to their reduced size dissimilar to those of large-scale equivalent [16,17]. Those nanoparticles can be produced by various physical and chemical methods [17,18]. Addition of nanoparticles to PVA membranes assists to modify their chemical and physical properties that include enhancing the x-ray attenuation [6].

Previously, we presented the production of composite membranes with controlled electrical conductivity based on PVA, and their different applications [14,15,19,20]. Several types of semiconducting metal-oxide nanoparticles were added to the membranes to control and

* Corresponding author at: Center for Sustainable Development, Qatar University, Doha, Qatar.
E-mail address: ayesh@qu.edu.qa (A.I. Ayesh).

https://doi.org/10.1016/j.apsusc.2020.146958
Received 5 May 2020; Received in revised form 5 June 2020; Accepted 11 June 2020
Available online 17 June 2020

design their characteristics based on the target applications [13,18,21–24]. Herein, we investigate the synthesis of CuO metal-oxide nanoparticles (NPs) and their incorporation with PVA + GL to produce flexible membranes of polymer-nanoparticles. The composition and structure of nanoparticles are examined. The mechanical, structural, and electrical properties of the PVA + GL + NPs membranes are explored in details. The x-ray response of the PVA + GL + NPs membranes is explored with variable x-ray generator voltage. The results presented here demonstrate a simplified and scalable fabrication process with reasonable cost of composite PVA + GL + NPs membranes that have potential of utilization for x-ray detection applications for various sectors [25,26].

2. Experimental:

2.1. Materials

$Cu(CH_3COOH)\cdot H_2O$ 99%, PVA (61,000 g/mol), ethanol 99.8%, glycerol with 99.5% purity, and NaOH were retrieved from Sigma Aldrich. Acetic acid 99.5% was purchased from BDH.

2.2. Synthesis of CuO nanoparticles

CuO nanoparticles were prepared according to our previous work [27] using a solvothermal method with some modification. 100 ml of ethanol solution, 0.36 g $Cu(CH_3COOH).H2O$, and 0.25 ml of acetic acid were placed in a round-bottom flask that was refluxed at 80 °C. Under vigorous stirring, 0.3 g of NaOH was added to solution. The black nanoparticles were formed and kept with stirring for 30 min. After cooling down, the nanoparticles were washed, with deionized water and alcohol, to remove any organic species using a centrifuge at 7000 rpm. The nanoparticles were re-dispersed in alcohol until used.

2.3. Fabrication of PVA-GL membranes

Polymer flexible membranes of PVA + GL + NPs were fabricated using a solution casting approach discussed in [9,13,15,19]. 10 g of coarse PVA was dissolved into 100 ml of double-distilled water by a magnetic stirrer. A PVA stock solution is produced with a weight concentration of 10%. 50 ml ethanol was introduced to the PVA solution after being cooled down to about 25 °C. A 5% GL solution in PVA was prepared at 60 °C with continuous magnetic stirring for 6 h. As a result, the PVA + GL solution was converted to a homogenous and clear product [14]. Precise weight concentrations of nanoparticles were presented to the PVA + GL solution while it was under magnetic stirring. The generated PVA + GL + NPs solution was then casted on glass substrates (Petri-dishes) and placed inside an oven at 70 °C overnight to vaporize the remaining solvents from the generated membranes. This process produced composite membranes (thin-films) of polymer-nanoparticles that are homogeneous, flexible, and with micro-thicknesses around 100 μm. The sheets of the membranes were produced with large size, thus, they were cut into specific sizes according to the requirements of the target tests.

2.4. Characterization

The crystal structure along with the composition of generated nanoparticles were examined using the x-ray diffraction (XRD) technique via a PANalytical system (model: Empyrean) [28]. The XRD tests were achieved by utilizing the Cu-K_α radiation peak with $\lambda = 1.5406$Å. The XRD diffraction scan was performed as a function of 2θ with a step size of 0.02° in the range $2\theta = 10.00 - 90.00^\circ$. A scanning electron microscope (SEM) (FEI, model: Nonva-NanoSEM-450) was utilized to investigate nanoparticle size and morphology. The SEM had an energy dispersive x-ray spectroscopy (EDS) attachment that allowed the investigation of nanoparticles' composition.

A model number Jade-DSC Differential Scanning Calorimeter (DSC) and model number Pyris6-TGA Thermal Gravimetric Analysis (TGA) systems of PerkinElmer made were employed to examine the melting point, stability, as well as indices of crystallinity for the membranes. The DSC tests were conducted with variable temperature within the range 20–250 °C, whereas the TGA tests were conducted in the range 20–700 °C using rate of heating of 10 °C/min. A spectrum-400-FT-IR/FT-NIR Fourier-transform infrared (FTIR) spectrometer of PerkinElmer systems was employed to inspect both vibration modes and structure of the composite and pure membranes. A DXR Raman spectrometer, made by Thermo Fisher Scientific, was employed to inspect membranes' crystallinity.

The electrical characteristics of the produced PVA + GL + NPs membranes were examined using an impedance spectroscopy technique by a 1260A impedance-gain-phase analyzer of Solartron. The spectroscopy tests were performed as a function of frequency (in the range $1.0 - 1.0 \times 10^6 Hz$) and temperature. The impedance measurements were established using a scheme where a membrane was inserted among a pair of metallic electrodes that were fixed on a temperature-controlled stage (a scheme of parallel-plate capacitor). A K-type thermocouple was positioned on the surface of the membrane to measure its temperature and control its heating process. Zview software of Scribner was employed to control the measurements via the impedance-gain-phase analyzer and to analyze the results. Herein, the software analyzed the electrical complex ac impedance ($Z(\omega)$) into its two components $Z'(\omega)$ and $Z''(\omega)$ that are real and imaginary, respectively. Both components are function of the angular frequency ω, here $\omega = 2\pi f$. Nyquist plots were generated to reveal the dependence of $Z''(\omega)$ on $Z'(\omega)$ with ω included as an implicit variable. A semicircle fitting was performed using Zview and utilized to determine the dc resistance and capacitance of the membranes. Furthermore, the semicircle fitting was utilized to conclude the equivalent circuit of the membrane-capacitor.

Fig. 1 demonstrates the setup used for x-ray response measurements [29,30]. In this setup, a membrane was inserted between copper and aluminum electrodes with the aluminum electrode facing x-ray. The x-ray was generated using a small x-ray source (educational XRD apparatus). The x-ray tube current was fixed at 1 mA, and the measurements were preformed as a function of x-ray tube voltage.

The mechanism in which the x-ray energy is converted into electrical current signal can be attributed to generation of free electrons inside a membrane by x-ray ionizing radiation. The free electrons generate electrical current that proportional to the x-ray dose. The x-ray electrical response was quantified using a unit of source measurement from Keithley Instruments (SMU-238), where a fixed voltage was applied across a membrane, and electrical current was evaluated upon variation of x-ray tube voltage.

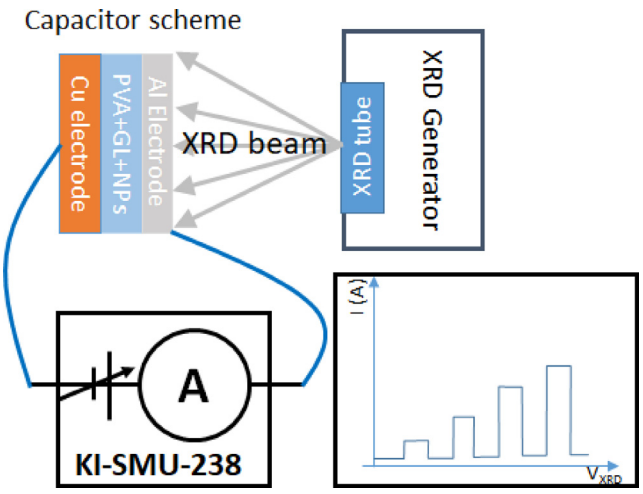

Fig. 1. Schematic diagram for the setup for x-ray response measurement.

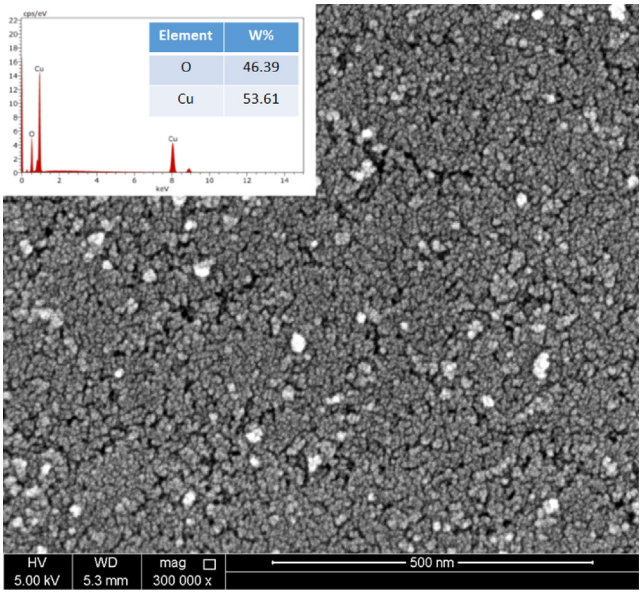

Fig. 2. SEM picture of the fabricated CuO nanoparticles. The inset in the picture is the EDS analysis.

3. Results and discussion

The nanoparticle size and morphology are identified by SEM. Fig. 2 presents an SEM image of the synthesized nanoparticles that reveals agglomeration of nanoparticles. The average individual nanoparticle size is $6.3 \mp 2.4nm$ with the uncertainty is the standard deviation. The inset in Fig. 2 reveals the composition of the nanoparticles as resolved by EDS, and it confirms the composition of CuO nanoparticles.

The structure and composition of CuO nanoparticles are also examined by XRD measurements and the results are presented in Fig. 3. The figure reveals the measured XRD spectrum as compared with the reference pattern and including its Miller indices [13,18,31]. The XRD analysis indicate that the nanoparticles exhibit monoclinic crystal structure with lattice parameters of $a = 4.6700$Å, $b = 3.4300$Å, and $c = 5.1200$Å. The XRD spectrum may be employed to evaluate the size ($2R$) of nanoparticles by Sherrer's equation [21,32]:

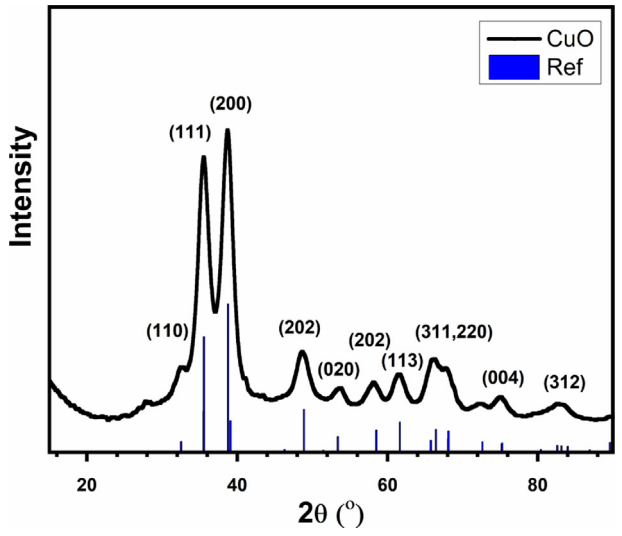

Fig. 3. XRD spectrum of the produced CuO nanoparticles. The lines represent the reference pattern.

$$2R = \frac{c\lambda}{\beta cos\theta}$$

where c is a dimensionless constant linked to the structure of nanoparticles (set at 0.95), λ is the wavelength of Cu-K_α radiation peak for XRD, and β (or FWHM) indicates the full-width-at-half-maximum for the selected XRD feature at the angle θ (known as the Bragg's angle). The nanoparticle size is evaluated using the (2 0 0) peak to 8.6 nm. The estimated size is consistent with the experimental size resolved from the SEM analysis within the range of error bars.

DSC measurements of the membranes are utilized to extract degree of crystallinity and to quantify the glass transition and melting temperatures, defined as T_g and T_m, respectively [33]. Fig. 4(a) demonstrates the results of DSC measurements of the composite membranes with different nanoparticle concentrations under a heating process between 30 and 250 °C. As the nanoparticle concentration increase, T_g shifts to lower temperatures in the range 70–100 °C which is due to nanoparticles inserted inside the lattice structure that make the crystalline domains of PVA to be relaxed. On the other hand T_m slightly shifts to lower temperatures in the range 205–218 °C with nanoparticle concentration due to CuO increase of heat adsorption of PVA, which is one of the unique properties of transition and noble metals.

TGA tests are applied to identify the lost mass, stability, and amount of loading for the membranes at variable nanoparticle concentration under heating process [34]. Fig. 4(b) demonstrates the TGA results with different stages upon ascendant of temperature from 30 to 650 °C. Rising the temperature from 30 to 100 °C result the adsorbed water to be removed which is bonded weakly to the membranes by hydrogen bonds. This stage is followed by elimination of hydroxyl group and volatile organic adsorbed, from 100 °C to the melting point at 200 °C. The degradation stage of chains starts from 200 °C for the composite membranes, and from 260 °C for the pure membrane, to about 380 °C due to PVA chain degradation. The stage from 380 to 600 °C is assigned to the carbonation. The TGA tests demonstrate the stability of the membranes towards heating since they are slightly affected with nanoparticles where the degradation stage is shifted slightly to lower temperatures.

Raman spectroscopy is applied to evaluate the influence of nanoparticle addition on crystal structure, i.e molecular vibrations of composite membranes. The results of Raman spectroscopy tests are presented in Fig. 5(a). The figure elucidates a peak at 2914 cm^{-1} that is attributed to the stretching vibration of CH^{2-} and a 1567 cm^{-1} peak that is assigned to the C═C and C—H stretching vibrations [31]. The intensity of the main peak drops and shifts to lower wavelengths with the increase in nanoparticle contents in the membranes, which means a decrease of crystallinity degree of PVA because of increasing nanoparticle concentration. It should be noted here that increasing nanoparticles concentration is observed to decrease the membrane flexibility and change its color to brownish-white instead of transparent.

FTIR measurements are applied to analyze the chemical and physical changes of PVA + GL + NPs membrane composites due to introduction of CuO nanoparticles. Fig. 5(b) presents FTIR spectra of PVA + GL + NPs membranes. The main broad peak shown in the figure is at 3268 cm^{-1} and it is ascribed to OH stretching bond. The intensity of the main peak declines with increasing the concentration of nanoparticles due to hydrogen bond between the nanoparticles and OH. The peaks at 2937 and 2914 cm^{-1} are ascribed to the vibration and stretching of CH^{3-} group. The other peaks at 1416 and 1089 cm^{-1} are due to the C-O bond. The peaks within the range 830–1150 cm^{-1} are related to C—O—C bond, while the peak at 1418 cm^{-1} is due to the CH2-CH3 bond. It should be noted that the physical properties, such as elasticity, are slightly reduced due to crosslinking between the nanoparticles and PVA, where glycerol is used to oppose this effect.

Impedance spectroscopy represents an outstanding tool to analyze the electrical properties of composite membranes. Herein, the electrical impedance is dependent on frequency and quoted as:

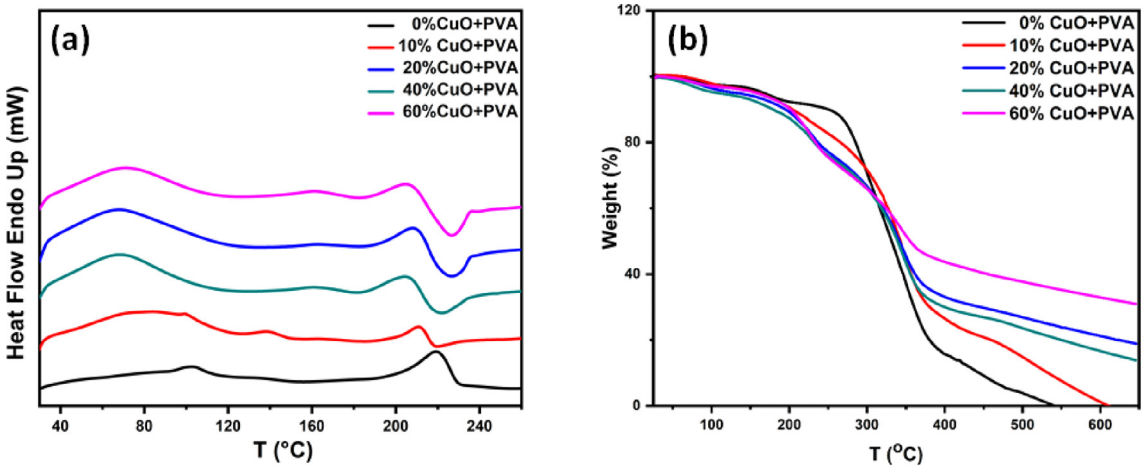

Fig. 4. (a) DSC and (b) TGA analysis of the PVA-CuO membranes at different concentrations (wt%) of nanoparticles.

$Z(\omega) = Z'(\omega) - iZ''(\omega)$

The real and imaginary elements of the impedance are illustrated using Nyquist plots wherein the frequency variable is implicit. Those plots presents the dependence as semicircular curves. $Z'(\omega)$ normally refers to the dc resistance (R) and it can be extracted from the radius of the semicircle in a Nyquist plot. Fig. 6 reveals the Nyquist plots of the fabricated PVA + GL + NPs membranes at different nanoparticle concentrations and temperatures. The figure reveals a general feature where the semicircle radius decrease as the temperature increases. This refers to the decrease of dc resistance with temperature that implies that the membranes exhibit negative temperature coefficient of the resistance. The $Z''(\omega)$ dependence on $Z'(\omega)$ can be employed predict the equivalent circuit of the PVA + GL + NPs membranes by fitting the curves using Zview software. Here, each semicircle represents a parallel pair of resistor and capacitor. Since all curves in Fig. 6 reveal single semicircle, each membrane can be represented by a circuit of parallel resistor and capacitor (single pair). The capacitor represents the influence of the electron depletion region, while the resistor refers to the effect of grain boundaries within the PVA + GL + NPs membranes. Both resistor and capacitor effects represent the kinetic charge transfer process at high frequencies and marginal movement of ions because of high relaxation time at low frequencies, respectively [20,35].

The resistance values of the different membranes cannot be compared due to their different thicknesses. Thus, the resistivity (ρ), that is independent of a membrane dimensions, is calculated for each membrane using $\rho = \frac{RA}{l}$, where l is the span of the membrane and A is the electrical contact area. The resistivity dependence on temperature ($ln(\rho) versus \frac{1000}{T}$) is presented in Fig. 7(a). The results in the figure are fitted using the Arrhenius dependence: $\rho = \rho_c e^{\frac{E_a}{k_B T}}$ with ρ_c is a temperature independent constant, k_B is the constant of Boltzmann, and E_a gives the activation energy. The solid lines in the figure represent linear fits to the Arrhenius equation. Other than the pure PVA + GL membrane, the figure demonstrates a decrease for the slope with increasing the concentration of nanoparticles. The activation energies are determined from the fits and presented in Fig. 7(b). The figure demonstrates an increase of the activation energy upon doping the membranes with nanoparticles, then, the activation energy decreases with nanoparticle concentration. This indicates that: i) the resistivity of both PVA + GL and PVA + GL + NPs are comparable, and ii) the ability to control the resistivity and activation energy of the membranes by addition of thorough amount of CuO nanoparticles. The increase of the resistivity for the membranes upon introducing 10% of nanoparticles (as compared with the pure PVA + GL) can be ascribed to the increase of charge scattering centers in the membranes upon addition of nanoparticles. However, decreasing the resistivity with nanoparticle concentration can be referred to the increase of CuO nanoparticles' concentration that exhibit a lower resistivity as compared with pure PVA + GL membranes. Beyond 10%, increasing nanoparticle concentration creates further charge transport baths within the membranes that lower both activation energy and resistivity. The response of the polymer membranes to x-ray is investigated with variable nanoparticle concentration and x-ray generator voltage (V_{XRD}) at a fixed x-ray tube

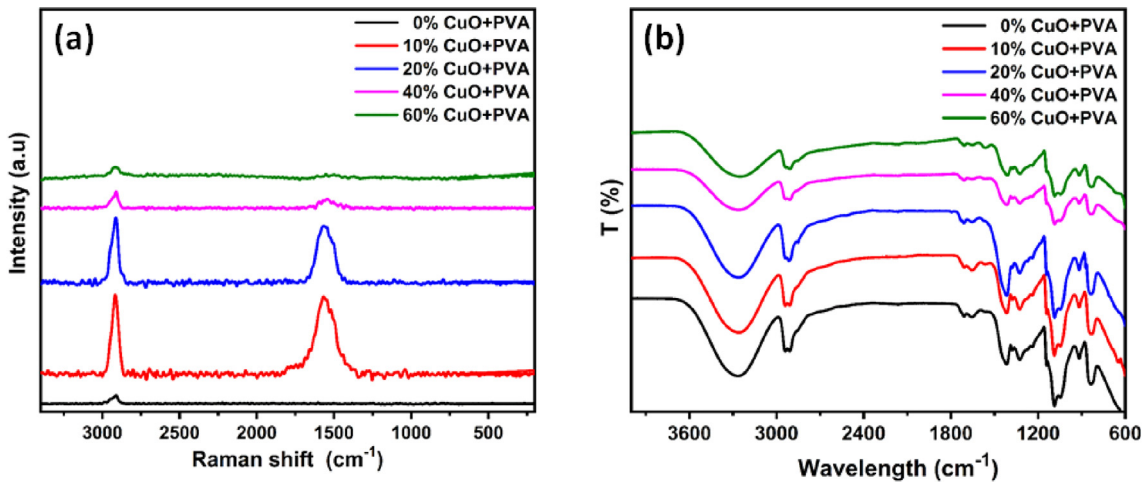

Fig. 5. (a) Raman and (b) FTIR analysis of the PVA-CuO membranes at different concentrations (wt%) of nanoparticles.

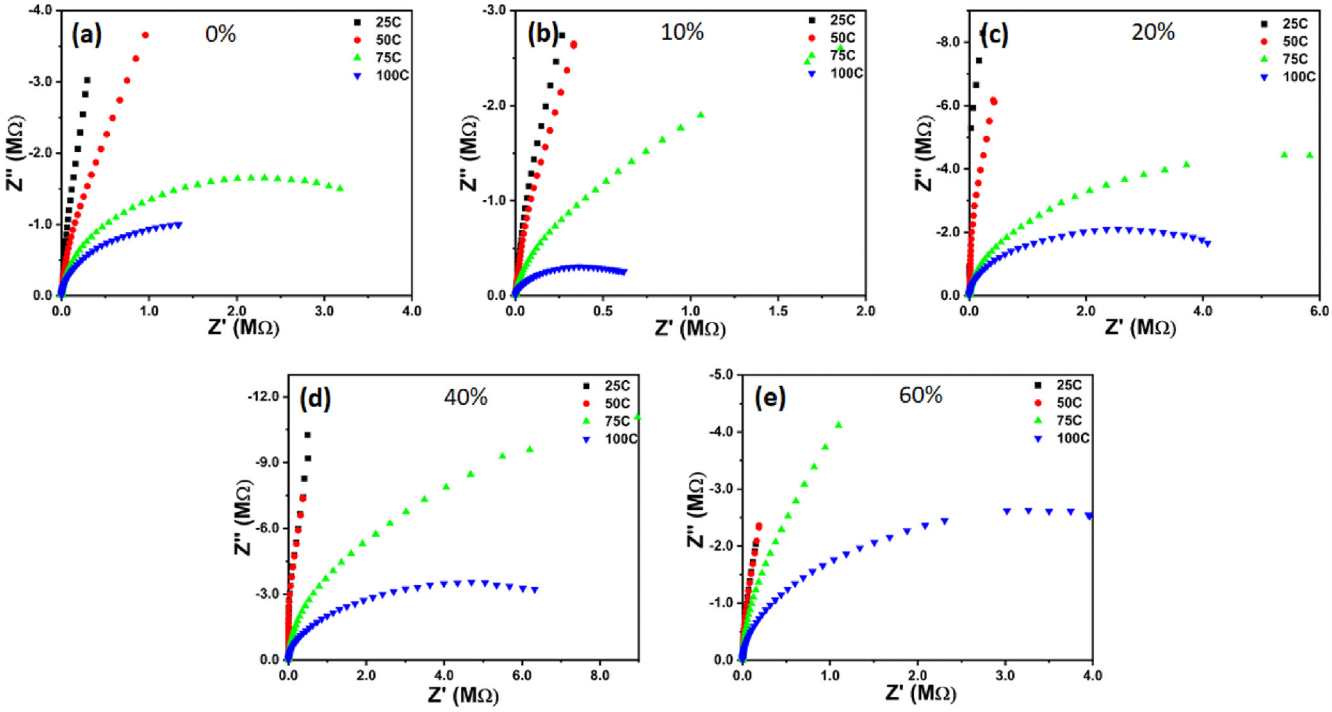

Fig. 6. Electrical impedance spectroscopy measurements of the produced PVA-CuO membranes at different nanoparticles' concentrations: (a) 0%, (b) 10%, (c) 20%, (d) 40%, and (e) 60%.

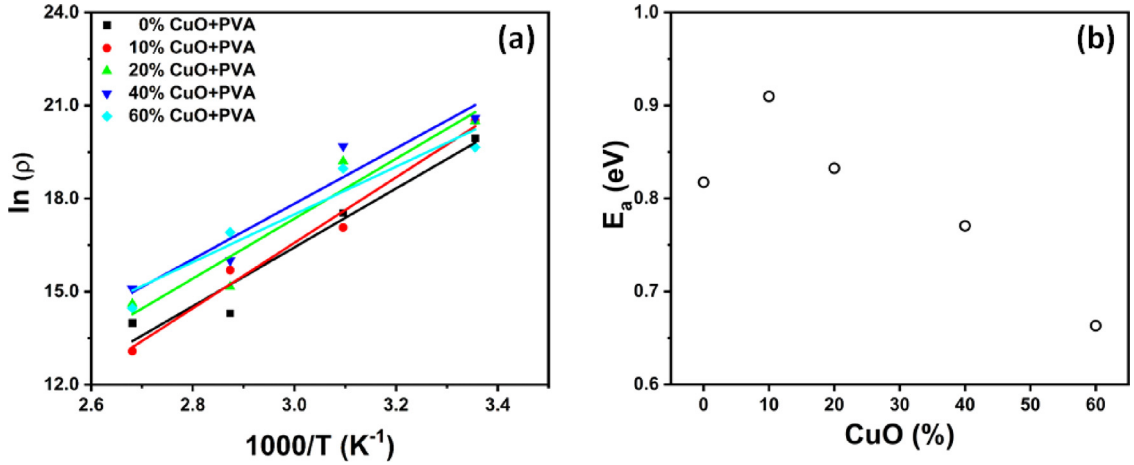

Fig. 7. a) The temperature dependence of the resistivity (natural logarithm) for the produced PVA-CuO membranes at different concentrations (wt%) of nanoparticles, and (b) the activation energy as a function of wt% concentrations of nanoparticles.

current of 1 mA. Fig. 8(a) reveals the change of electrical current response, measured at a fixed dc bias across each membrane of 50 V, with V_{XRD} and nanoparticle concentration of the membranes. The electrical current response here is defined as $\frac{\Delta I}{I_0}$, where ΔI is the current change $I - I_0$ and I_0 is the base current value. The figure illustrates that the current response increases with increasing V_{XRD} and nanoparticle concentration of the membranes (up to 40%). The dependence of the current response on $V_{XRD}$is presented in Fig. 8(b). For the pure PVA + GL, no response to x-ray is observed which indicates that the x-ray response is assigned to the nanoparticles. The PVA + GL + NPs with 40% nanoparticle concentration exhibits the best x-ray response (about 4 times of 10% at $V_{XRD} = 35kV$). The low x- ray response of the PVA + GL + NPs with 60% nanoparticle concentration maybe assigned to the effect of reduced crystallinity of PVA due to the high concentration of nanoparticles that create further scattering cites for the generated electrons by x-ray. The illustrated results demonstrate the potential for implementation of the present PVA + GL + NPs membranes for x-ray detection applications.

4. Conclusion

Flexible composite polymer-nanoparticles membranes were prepared for the applications of x-ray detection. The composite membranes consist of: poly(vinyl alcohol) (PVA) that represent the polymer matrix, glycerol (GL) plasticizer to improve the flexibility and electrical conductance of the membranes, and different concentrations of CuO nanoparticles. The CuO nanoparticles were made using a solvothermal method, and mixed with the PVA + GL solution to generate flexible membranes by solution casting. The nanoparticles exhibit a grain size of $6.3 \mp 2.4nm$. X-rad spectroscopy confirmed the composition of the synthesized nanoparticles with a monoclinic crystal structure. Addition of nanoparticles to the polymer membranes was found to decrease both

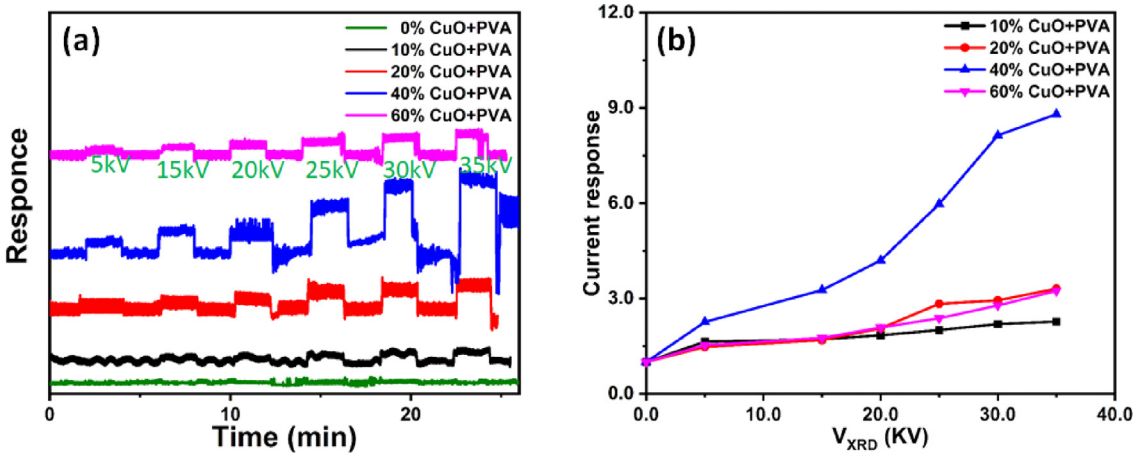

Fig. 8. a) The current response with XRD generator voltage (fixed XRD generator current of 1 mA). (b) The variation of current response with XRD generator voltage.

melting and glass transition temperatures of PVA. The degradation temperature of the membranes was affected slightly due to introduction where it was shifted to lower temperatures. Furthermore, addition of nanoparticles to the membranes had minimal effect on their flexibility. Impedance spectroscopy measurements demonstrated a negative temperature coefficient of resistance for the membranes wherein the resistance decrease with increasing the temperature. The membrane's activation energy decreased with nanoparticle concentration since CuO nanoparticles exhibit low resistivity compared with PVA. The dependence of x-ray response on x-ray generator voltage for the membranes was tested. The results indicated that x-ray response of the membrane was owing to CuO nanoparticles, where increasing nanoparticle concentration (up to 40%) increased the x-ray response. The present membranes exhibit many advantages where they hold semiconducting features, flexible, and practical to fabricate at large scale. This indicates that those membranes can be considered as potential candidates of the applications of x-ray detection.

CRediT authorship contribution statement

Ahmad I. Ayesh: Conceptualization, Data curation, Formal analysis, Funding acquisition, Investigation, Methodology, Project administration, Resources, Software, Supervision, Validation, Visualization, Writing - original draft, Writing - review & editing. **Belal Salah:** Data curation, Investigation. **Rama Nawwas:** Data curation, Investigation. **Aldana Alyafei:** Data curation, Investigation. **Sara AlMansouri:** Data curation, Investigation. **Leena Al-Sulaiti:** Conceptualization, Resources, Writing - review & editing.

Declaration of Competing Interest

The authors declare that they have no known competing financial interests or personal relationships that could have appeared to influence the work reported in this paper.

Acknowledgements

This work was supported by Qatar National Research Fund under grant number, UREP24-015-2-007. The FTIR, Raman, DSC, TGA, SEM, and EDS measurements were accomplished in the Central Laboratories unit at Qatar University. The publication of this article was funded by the Qatar National Library.

References

[1] H. Tsai F. Liu S. Shrestha K. Fernando S. Tretiak B. Scott D.T. Vo J. Strzalka W. Nie A sensitive and robust thin-film x-ray detector using 2D layered perovskite diodes, Science Advances 6 2020 eaay0815.
[2] A. Cowen, S. Kengyelics, A. Davies, Solid-state, flat-panel, digital radiography detectors and their physical imaging characteristics, Clin. Radiol. 63 (2008) 487–498.
[3] K. Wells, D. Bradley, A review of X-ray explosives detection techniques for checked baggage, Appl. Radiat. Isotopes 70 (2012) 1729–1746.
[4] A. Bergamaschi, S. Cartier, R. Dinapoli, D. Greiffenberg, I. Johnson, D. Mezza, A. Mozzanica, B. Schmitt, X. Shi, J. Jungmann-Smith, X-ray detector development at the Swiss Light Source, Synchrot. Radiat. News 27 (2014) 3–8.
[5] A.I.a.C.A.M.a.M.S.a.P.J.S.a.J.L. Keddie, Heavy metallic oxide nanoparticles for enhanced sensitivity in semiconducting polymer x-ray detectors Nanotechnology 23 2012 235502.
[6] C.A. Mills, H. Al-Otaibi, A. Intaniwet, M. Shkunov, S. Pani, J.L. Keddie, P.J. Sellin, Enhanced x-ray detection sensitivity in semiconducting polymer diodes containing metallic nanoparticles, J. Phys. D Appl. Phys. 46 (2013) 275102.
[7] A.C. Obreja, D. Cristea, R. Gavrila, V. Schiopu, A. Dinescu, M. Danila, F. Comanescu, Isocyanate functionalized graphene/P3HT based nanocomposites, Appl. Surf. Sci. 276 (2013) 458–467.
[8] M. Alba-Martin, T. Firmager, J. Atherton, M.C. Rosamond, D. Ashall, A.A. Ghaferi, A. Ayesh, A.J. Gallant, M.F. Mabrook, C. Petty, D.A. Zeze, Improved memory behaviour of single-walled carbon nanotube charge storage nodes, J. Phys. D Appl. Phys. 45 (2012) 295401.
[9] A.I. Ayesh, S. Qadri, V.J. Baboo, M.Y. Haik, Y. Haik, Nano-floating gate organic memory devices utilizing Ag-Cu nanoparticles embedded in PVA-PAA-glycerol polymer, Synth. Met. 183 (2013) 24–28.
[10] M.Y. Haik, A.I. Ayesh, T. Abdulrehman, Y. Haik, Novel organic memory devices using Au–Pt–Ag nanoparticles as charge storage elements, Mater. Lett. 124 (2014) 67–72.
[11] A.F.S. Abu-Hani, F. Awwad, Y.E. Greish, A.I. Ayesh, S.T. Mahmoud, Design, fabrication, and characterization of low-power gas sensors based on organic-inorganic nano-composite, Org. Electron. 42 (2017) 284–292.
[12] Y. Sakurada, A. Sueoka, M. Kawahashi, Blood purification device using membranes derived from poly (vinyl alcohol), and copolymer of ethylene and vinyl alcohol, Polym. J. 19 (1987) 501–513.
[13] A.I. Ayesh, A.F.S. Abu-Hani, S.T. Mahmoud, Y. Haik, Selective H2S sensor based on CuO nanoparticles embedded in organic membranes, Sens. Actuat. B 231 (2016) 593–600.
[14] M. Allam, A.I. Ayesh, M.A. Mohsin, Y. Haik, Physical Properties of PVA Doped with Algal Glycerol, J. Appl. Polym. Sci. 130 (2013) 4482–4489.
[15] V. Josh, M.Y. Haik, A.I. Ayesh, M.A. Mohsin, Y. Haik, Electrical properties of sorbitol doped PVA-PAA polymer membranes, J. Appl. Polym. Sci. 128 (2012) 3861–3869.
[16] A.I. Ayesh, Electronic transport in Pd nanocluster devices, Appl. Phys. Lett. 98 (2011) 133108.
[17] A. Ayesh, N. Qamhieh, H. Ghamlouche, S. Thaker, M. El-Shaer, Fabrication of size-selected Pd nanoclusters using a magnetron plasma sputtering source, J. Appl. Phys. 107 (2010) 034317.
[18] S. Dagher, Y. Haik, A.I. Ayesh, N. Tit, Synthesis and optical properties of colloidal CuO nanoparticles, J. Lumin. 151 (2014) 149–154.
[19] Y. Haik, A.I. Ayesh, M. Allawy, Semiconducting polymer, in: U.S.P. Application (Ed.), 2014.
[20] A.I. Ayesh, M.A. Mohsin, M.Y. Haik, Y. Haik, Investigations on electrical properties of poly(vinyl alcohol) doped with 1-methyl-3-n-decyl-imidazolium bromide ionic liquid, Curr. Appl Phys. 12 (2012) 1223–1228.
[21] M.A. Haija, A.I. Ayesh, S. Ahmed, M.S. Katsiotis, Selective hydrogen gas sensor using CuFe2O4 nanoparticle based thin film, Appl. Surf. Sci. 369 (2016) 443–447.
[22] A.I. Ayesh, S.T. Mahmoud, N. Qamhieh, Z.A. Karam, Investigation of charge transport in percolating network of PdCu nanoclusters, Acta Metall. Sin. 27 (2014) 156–160.
[23] S. Dagher, A.I. Ayesh, N. Tit, Y. Haik, Influence of reactant concentration on optical properties of ZnO nanoparticles, Mater. Technol. 29 (2014) 76.
[24] A.I. Ayesh N. Qamhieh H. Ghamlouche a.M.E.-S. S. Thaker, Fabrication of size-

selected Pd nanoclusters using a magnetron plasma sputtering source J. Appl. Phys. 107 2010 034317.
[25] S.A. Nouh, A. Abdel Naby, P.J. Sellin, Modification induced by proton irradiation in Makrofol-DE polycarbonate, Radiat. Meas. 42 (2007) 1655–1660.
[26] A. Intaniwet, J.L. Keddie, M. Shkunov, P.J. Sellin, High charge-carrier mobilities in blends of poly(triarylamine) and TIPS-pentacene leading to better performing X-ray sensors, Org. Electron. 12 (2011) 1903–1908.
[27] A.I. Ayesh, A.A. Alyafei, R.S. Anjum, R.M. Mohamed, M.B. Abuharb, B. Salah, M.J. A.P.A. El-Muraikhi, Production of sensitive gas sensors using CuO/SnO 2 nanoparticles, 125 (2019) 550.
[28] A.I. Ayesh, M.A. Haija, A. Shaheen, F. Banat, Spinel ferrite nanoparticles for H2S gas sensor, Appl. Phys. A 123 (2017) 682.
[29] A.I. Ayesh, B. Salah, L.A. Al-Sulaiti, Production and characterization of flexible semiconducting polymer-nanoparticle composites for x-ray sensors, Radiat. Phys. Chem. 167 (2020) 108233.
[30] L.A. Al-Sulaiti, B. Salah, A.I. Ayesh, Investigation of flexible polymer-Tl2O3 nanocomposites for x-ray detector applications, Appl. Surf. Sci. 489 (2019) 351–357.
[31] A.I. Ayesh, A.A. Alyafei, R.S. Anjum, R.M. Mohamed, M.B. Abuharb, B. Salah, M. El-Muraikhi, Production of sensitive gas sensors using CuO/SnO 2 nanoparticles, Appl. Phys. A 125 (2019) 550.
[32] A.R. Said, K. Said, F. Awwad, N.N. Qamhieh, S.T. Mahmoud, M.A. Meetani, S. Tariq, A.I. Ayesh, Design, fabrication, and characterization of Hg2+ sensor based on graphite oxide and metallic nanoclusters, Sens. Actuat. A-Phys. 271 (2018) 270–277.
[33] O.W. Guirguis, M.T. Moselhey, Thermal and structural studies of poly (vinyl alcohol) and hydroxypropyl cellulose blends, Nat. Sci. 4 (2012) 57.
[34] C.-C. Yang, W.-C. Chien, Y.J. Li, Direct methanol fuel cell based on poly (vinyl alcohol)/titanium oxide nanotubes/poly (styrene sulfonic acid)(PVA/nt-TiO2/PSSA) composite polymer membrane, J. Power Sour. 195 (2010) 3407–3415.
[35] O.K. Varghese, L. Malhotra, Studies of ambient dependent electrical behavior of nanocrystalline SnO 2 thin films using impedance spectroscopy, J. Appl. Phys. 87 (2000) 7457–7465.